Organic Field-Effect Transistor/Memory Devices with Pentacene/Polydiacetylene Composite Film As Active Channel Material: A Morphology Dependence Study

Chiao-Wei Tseng[†,‡] **and Yu-Tai Tao**[*,†,‡]

Institute of Chemistry, Academia Sinica, Taipei, Taiwan, and Department of Chemistry, National Tsing-Hua University, Hsin-chu, Taiwan

ABSTRACT Composite films of pentacene and poly(10,12-pentacosadiynoic acid) were prepared and used as the active channel material in a top-contact, bottom-gate field-effect transistor. The transistors exhibited high field-effect mobility as well as large $I-V$ hysteresis as a function of gate bias history. The polydiacetylenic moieties incorporated in the pentacene film served as charge storage vehicles, which affected the threshold voltage shifts and created the electric bistability needed in a memory device. The memory window, response, and retention highly depend on the morphology of the polydiacetylene film buried under. Detailed film structure analyses and correlation with the transistor/memory property are provided.

KEYWORDS: organic memory device • organic field effect transistor • pentacene • polydiacetylenes

INTRODUCTION

Organic materials have attracted much attention for building various components in electronic devices including displays, transistors, memories, switches, etc., much because of the potential advantages of the low-cost fabrication, light weight, and mechanical flexibility that organic materials can offer (1). Numerous efforts have been devoted to designing and incorporating organic materials into all of these components, because the properties of organic materials in general can be tailored to meet what is required in each application through rational design and chemical synthesis. For memory devices, an electric bistability is required so that information can be stored by encoding "0" and "1" on the basis of different electric responses (for example, conductivity) of the same material at a specific voltage.

Organic memory devices have been demonstrated in a diode architecture where metal nanoclusters (NCs) were embedded into an organic semiconducting layer in a triple layer (organic/metal NCs/organic, OMO) configuration to create the electric bistability states (2). The possible mechanism through which the memory effect works has been proposed to be through charge injection (triggered by a high voltage pulse) into and charge cancellation (by opposite voltage pulse) from the NCs so that the space charge field causes a dramatic change in the conductivity through the film. Three-terminal memory device has also been demonstrated using a transistor structure (3−6). The electric bistability state is reached by polarization switching or charge carriers trapping/detrapping in the dielectric layer through the action of gate bias to modulate the conductivity through the channel layer. Alternatively, metal nanoparticles have also been shown to function as hole traps when embedded into the conduction channel of a pentacene film-based transistor (7−10). Although the presence of metal nanoparticles much perturbs the crystallinity of pentacene film, a rational design of the nanoparticle/SAM system enables the use of them as a floating gate in the transistor/memory device while maintaining high efficiency transistor as well as a large memory window (9).

In light of the charge-trapping role played by metal nanoparticles in the transistor/memory device, a system with organic carrier traps inside the conducting channel would be interesting. While donor-type or acceptor-type organic moieties can be expected to trap mainly holes or electrons respectively, an extended conjugated system which can delocalize both positive charges and negative charges should be a promising candidate for the purpose of charge trapping. This has not been reported before.

Organic diacetylenic molecules, when in crystalline state with right relative orientation of neighboring diacetylenic units, are known to undergo topochemical polymerization reaction upon thermal or photochemical treatment, yielding alternating ene-yne conjugate systems while retaining nearly the same packing of the original crystal (11). The polydiacetylenes possess unique electro-optical properties that spark great interests in exploring the application of these materials in chemical and biological sensors, electronics, etc. (12−15). As the material has an extended conjugated system with highest occupied molecular orbital (HOMO) energy level

* Corresponding author. E-mail: ytt@chem.sinica.edu.tw.
Received for review August 5, 2010 and accepted October 12, 2010
† Academia Sinica.
‡ National Tsing-Hua University.
DOI: 10.1021/am100696v

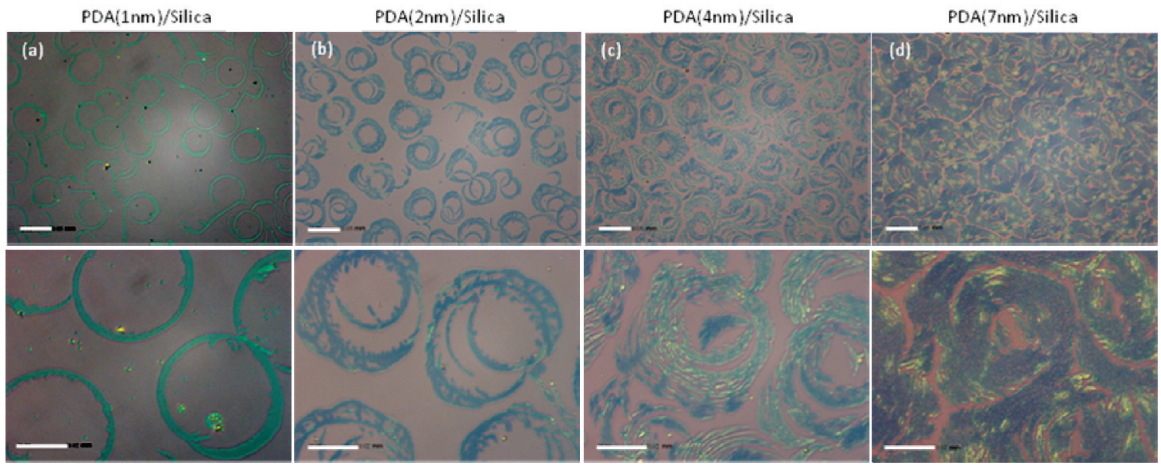

FIGURE 1. Optical micrographs of PDA films prepared by thermal evaporation on a bare silica up to a nominal thickness of (a) 1, (b) 2, (c) 4, and (d) 7 nm.

of ~5.2 eV and a lowest unoccupied molecular orbital (LUMO) at ~3.4 eV, which are in close disposition with the HOMO/LUMO levels of pentacene (5.1 and 2.9 eV, respectively) (16), charge carrier hopping between pentacene and the polymer system under the influence of a gate bias is possible. The alkyl chains surrounding the ene−yne backbone can be a tunneling barrier for the carrier hopping. This barrier is important in holding the charges necessary for the state switching (2). It is envisaged that by incorporating nanoclusters of polydiacetylenes in a pentacene film as charge-storing vehicles, a transistor/memory device may be expected.

In this work, a composite film of pentacene/poly(10,12-pentacosadiynoic acid, PDA) was prepared on a SiO_2 surface and used as the active channel material in a thin film transistor. The studies show that (1) depending on the surface character (bare or silane monolayer-covered), the PDA molecules self-assembled into distinct clusters/patterns of perpendicularly oriented H-bonded dimer layers; (2) UV-irradiation of the clusters/patterns generated oriented nanofibers of polyPDA; (3) the transistor based on the pentacene/polyPDA composite film prepared by depositing pentacene onto the polyPDA system exhibited high field-effect mobility (~0.2−2 $cm^2/(V\,s)$) as well as a clear electric bistability, that is, hysteresis in source/drain current as a function of applied gate voltage, with wide memory windows (~70−150 V); (4) the response and stability of the memory effect relate to the morphology of polyPDA obtained on different substrates. The potential for these polyPDAs to serve as floating gate in a transistor/memory application is demonstrated.

EXPERIMENTAL SECTION

Pentacosa-10,12-diynoic acid (PDA), *n*-hexacosane, and *n*-octadecyltrichlorosilane (OTS) were obtained commercially. *n*-Type silicon (100) substrate covered with 300 nm-thick, thermally grown oxide layer was cleaned by Piranha (70% H_2SO_4:30% H_2O_2) solution and thoroughly rinsed with pure water and dried by a stream of N_2. OTS-modified silicon substrate was prepared by immersing the cleaned substrate in a 1% (w/w) toluene solution of OTS for 3 min, followed by sonicating in pure toluene and blowing dry with N_2. The PDA films were prepared by depositing the monomers in a vacuum of 2×10^{-6} Torr and at a rate of 0.1 Å/s on a substrate kept at ambient condition up to various nominal thicknesses. Polymerization was carried out by using a UV lamp (wavelength 254 nm) with an intensity of 4 mW cm^{-2} for 5 min in air immediately after the sample was taken out of the vacuum chamber. Sixty nanometers of pentacene were thermally deposited (at a deposition rate of 0.2 Å/s) on the PDA-decorated substrate. Source and drain electrodes were deposited through a shadow mask to achieve a top-contact FET device with a channel length of 50 μm and a channel width of 500 μm.

Raman spectroscopy measurements were performed on a micro-Raman setup (Jobin-Yvon) with an argon-ion laser at 514.5 nm, and the dispersed spectra were recorded by a liquid-N_2-cooled charge-coupled device (CCD) camera. A low laser power density was used for the measurement to prevent local heating and decomposition of PDAs. The near-edge X-ray absorption fine structure (NEXAFS) spectra were taken at the X-ray photoemission microscopy station at National Synchrotron Radiation Research Center (NSRRC), Taiwan. The radiation with an energy resolution of 100 meV at the carbon K-edge and a focused spot size of 0.1 × 1 mm^2 was delivered to the sample. Atomic force microscopy analyses were carried out with a Multimode Atomic Force Microscope (Digital Instruments, Nanoscope III) using tapping mode with a silicon tip. The powder X-ray diffraction measurements were carried out with a Philips X'Pert diffractometer equipped with an X'Celerator detector. The electrical characteristics of the transistor devices were measured in ambient with a HP4156 parameter analyzer.

RESULTS AND DISCUSSION

Characterization of the PDA Films. Attenuated total reflectance infrared spectrum of a thicker deposited and UV-irradiated film (60 nm) showed methylene stretches at 2920 and 2849 cm^{-1} for $\nu_{as}(CH_2)$ and $\nu_s(CH_2)$, respectively, and the carboxyl stretch at 1689 cm^{-1}. These characteristics are similar to that of the bulk crystalline PDA sample. A strong UV absorption band near 600 nm was observed, as expected for the polydiacetylenes (10, 17). The most distinct feature lies in the film morphology at low thickness. The optical micrographs (Figure 1) show that at 1 nm nominal thickness, numerous isolated rings were formed, with a similar diameter of ~50 μm and similar width of ~5 μm. With increasing nominal film thickness, the ring-shaped structure is maintained, with growing ring width. Thus rings of specific dimension were formed, followed by expansion

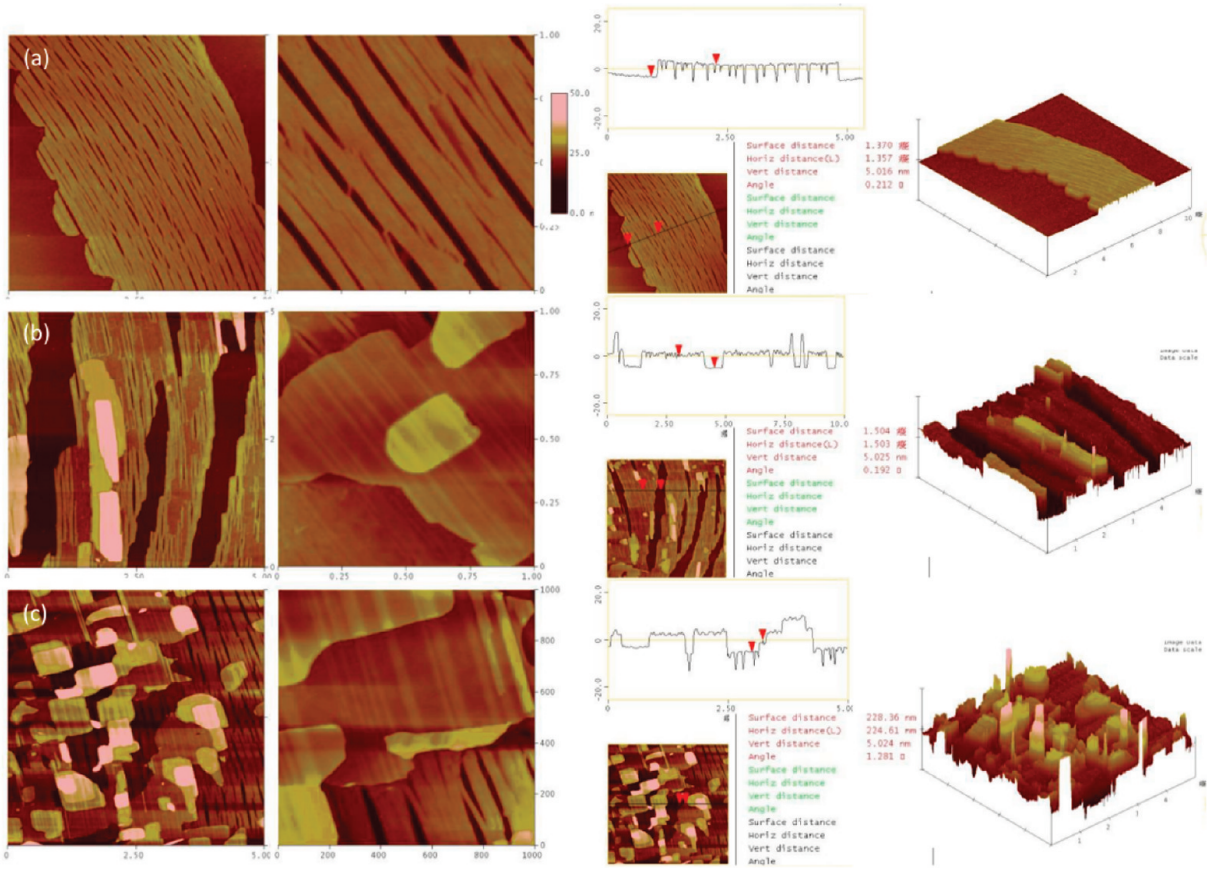

FIGURE 2. AFM topographic images (left, 5 μm × 5 μm, right 1 μm × 1 μm, 100 nm in height), corresponding line profiles, and 3D images of polyPDA films with a nominal thickness of (a) 1, (b) 4, and (c) 7 nm.

in the width. AFM analysis gives further details of the films (Figure 2). At 1 nm thickness, the rings appear to compose of numerous fibers roughly oriented along the peripherals of the rings. Some crossover of the fibers is observed. The fibers are all of similar heights of ~5 nm. On the basis of the length of a stretched PDA molecule (~3.1 nm), the nearly uniform height of ~5 nm suggests a dimeric layer of stretched PDA molecules at a finite inclination angle of ~36° from the surface normal.

The closer-to-normal orientation of the dimer moieties is also supported by the near edge X-ray absorption fine structure (NEXAFS) measurements, which showed an opposite trend in the intensities of core to σ^* (C−C) transition at 294.8 eV and core to σ^*(C−H) transition at 288.7 eV as a function of incidence angle at 90 and 20° respectively, due to the near orthogonal orientation of the C−C and C−H bonds (see Figure S1 in the Supporting Information). Similar inclination angle has been reported in a Langmuir film of PDA prepared at the air/water interface, which polymerizes to yield polydiacetylenes of different phases (18). As the nominal thickness increased, the average width of the ring increased, together with some scattered and terraced patches on the 5 nm thick films, also ~5 nm in height (Figure 2b). At a thickness of 7 nm (Figure 2c), the surface was almost filled up with the dimer layers. The ring patterns are still discernible. Raman spectra of the polyPDA films showed distinct peaks at 1135, 1520, and 2120 cm^{-1}, which are attributable to the stretching modes of a C−C bond, a C═C bond, and a C≡C bond, respectively (19, 20), in agreement with an alternating ene−yne conjugated backbone in the polymer. The peak intensity increased with increasing thickness. At a thickness of 7 nm, a new peak at 1457 cm^{-1} can be seen (see Figure S2 in the Supporting Information). Shift of the C═C stretch mode to lower wavenumbers has been suggested for more extended conjugated systems (14). From the spectroscopic data and the AFM images, it is proposed that the acid molecules, upon thermal deposition, migrated on the silica surface and nucleated to form H-bonded dimers and grew faster along one direction to form nearly linear packing. This direction is suggested to be the direction of the plane containing the trans zigzag carbon chain, along which has more favorable van der Waal interactions (21). However, the near linear growth eventually looped up over a long distance. The ring formation is suggested to be due to a slight chain twist in optimizing the chain−chain interaction, which leads to a curved growth over a long distance (with a diameter of ~50 μm). Film growth in the direction perpendicular to the trans plane was slower, giving the thin width of the ring. With more molecules arriving at the substrate, they packed along the edge of the ring so that the width of the ring increased, until the surface was mostly filled with the dimer layers. UV-irradiation resulted in polymerization along the trans plane direction and gave the fibrillar structure along the ring. The process is depicted in Figure 3.

The oriented polymerization is supported by the polarization-dependent micro- Raman spectroscopy, which showed

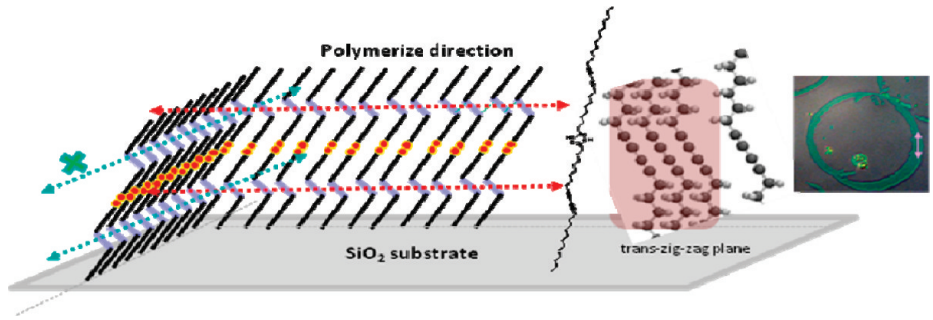

FIGURE 3. Schematic diagram showing the growth of PDA monomers on a bare silica substrate. The arrows show the direction of polymerization.

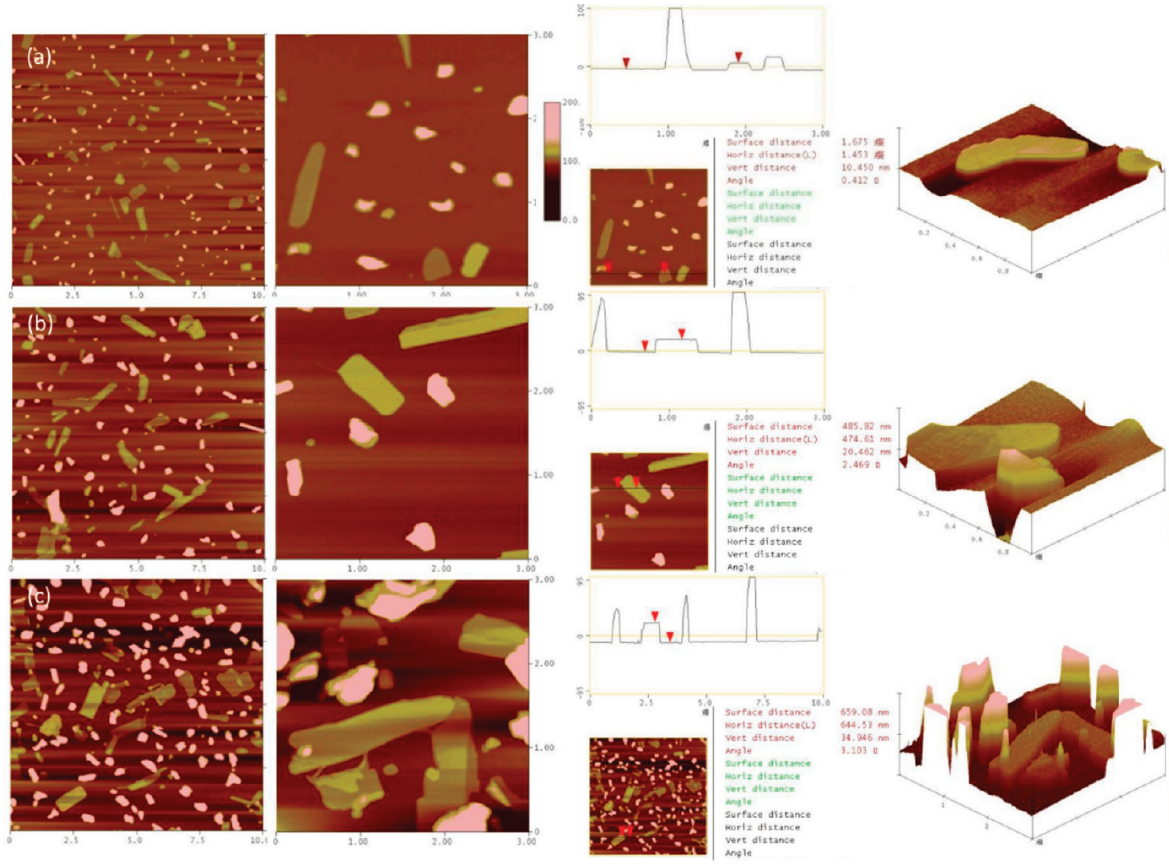

FIGURE 4. AFM topographic images (left, 10 μm × 10 μm; right, 1 μm × 1 μm; 200 nm in height), corresponding line profiles, and 3D images of polyPDA clusters deposited on OTS-modified silica surface with a nominal thickness of (a) 2, (b) 4, and (c) 7 nm.

much enhanced absorption peak intensity for the conjugated ene−yne backbone along tangential direction versus the radial direction (see Figure S3 in the Supporting Information).

The HOMO levels in these films were measured by X-ray photoemission spectroscopy (AC2). Depending on the thickness, the HOMO value changed slightly, from 5.41 to 5.32 eV to 5.28 eV for 1, 3, and 7 nm films, respectively. The slight increase in the HOMO energy level with increasing film thickness could imply an increase in the conjugation or the order of the polymer films for thicker films. This is in corroboration with the appearance of a peak at 1457 cm^{-1} in Raman spectrum mentioned above, where a more extended conjugation was suggested.

PDA films were also deposited on *n*-octadecyltrichlorosilane(OTS)-modified silica surface, a common substrate used to render hydrophobicity to the surface and improve the field-effect mobility of the thin film transistors (22−25). A totally different morphology was obtained. No ring patterns were found. Rather, clusters of irregular sizes and different heights were obtained (Figure 4). Section analysis shows that even at a nominal thickness of 2 nm, the sizes of the clusters are found to be submicrometer in width but multiples of ~5 nm in height, suggesting piles of dimer layers were obtained. The drastic morphology difference between films on the bare silica and the OTS-covered silica can be attributed to surface energy and/or roughness factor. Aggregation is favored on a lower surface energy substrate and OTS-modification renders a lower surface energy on silica (26). Yet there are some complications in the effect of surface energy on the grain sizes, because the organic monolayer lowers the surface energy but also introduces cohesive

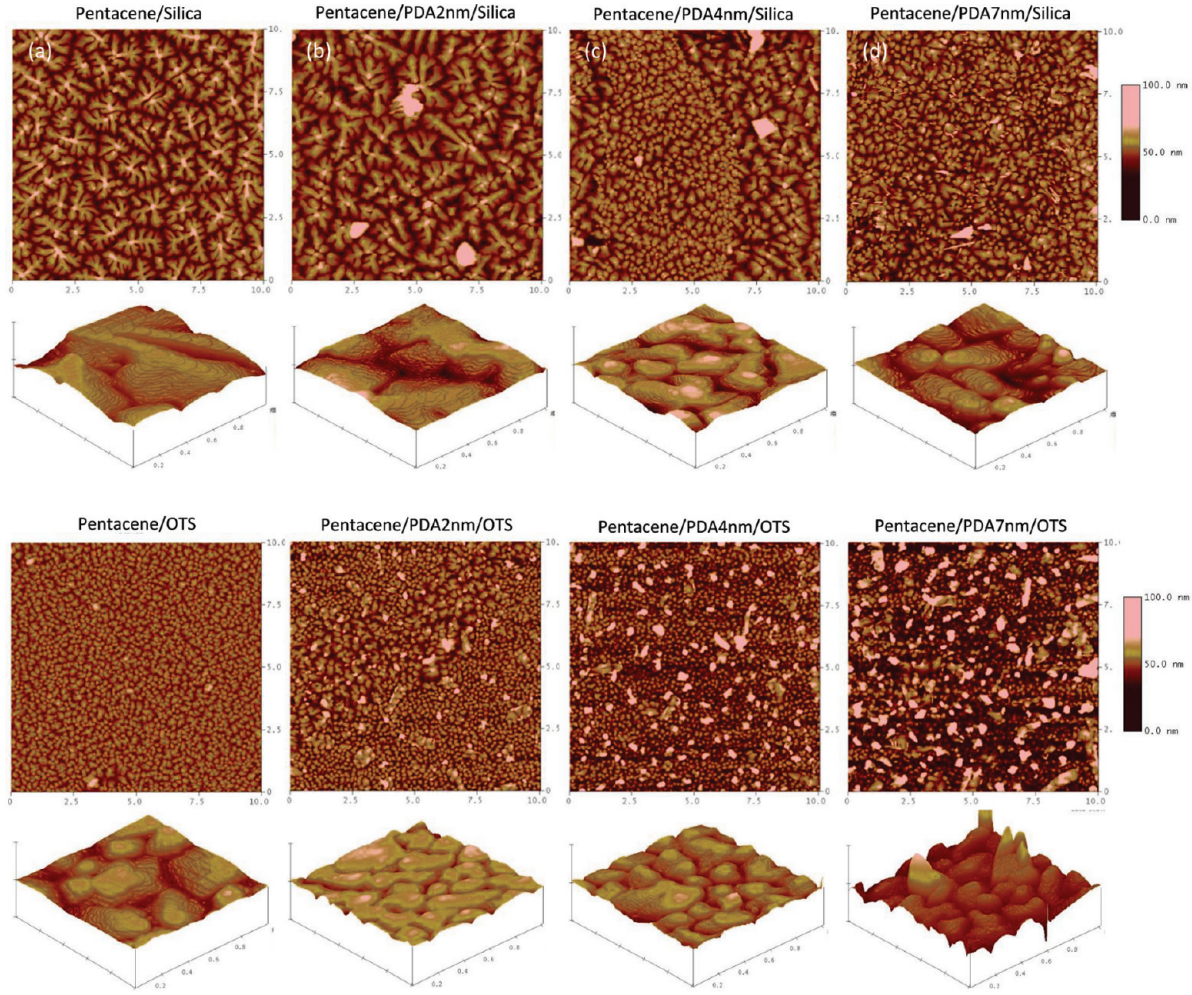

FIGURE 5. AFM micrographs (10 μm × 10 μm, 100 nm in height) of 60-nm pentacene films deposited on (a) a bare silica and polyPDA-covered silica substrates, (b) OTS-silica and polyPDA-covered OTS-silica substrate. The nominal polymer thicknesses are 2 nm, 4 nm, and 7 nm respectively. The corresponding 3D images are 1 μm × 1 μm in size.

interaction with the organic molecules deposited on top (27, 28). The effect of surface roughness can also contribute. Because of the multidomain nature of the two-dimensional solid-state monolayer (29), molecular domain boundaries and defects in the monolayer provide the nucleation sites where deposited molecules can get trapped. Lower surface diffusion and thus smaller grains were obtained because of these nucleation sites. The grain reduction observed when pentacene was deposited on as-adsorbed OTS-monolayer surface compared to bare silica surface can be the result of increased molecular interaction and roughness (20, 30).

It is also interesting to note that on an OTS-modified surface, multilayers (tetra-, hexa-layers and higher) were formed even at very low PDA surface coverage, whereas on a bare silica surface, the multilayer patches started to form after the surface was mostly covered by the dimer layers. The bare silica has a higher surface energy and the dimer layer films are exposing a lower energy surface (with a water contact ~97° obtained on the 7 nm PDA-covered surface). The OTS-modified silica also has a low surface energy, similar to the dimer film areas. Thus the results suggest the dimer moieties tend to grow on the bare and higher surface energy areas in the former case but nonselectively on the OTS-modified surface and the dimer layer-covered regions, or even more preferentially on the dimer layer-covered regions. Here we suggest the role of surface roughness sets in: on areas where the surface energies are similar, the dimers reside on rougher areas preferentially. AFM analysis showed that the dimer fibers-covered areas are much rougher (a rms roughness ~2.1 nm) than the OTS-modified areas (rms roughness ~0.21 nm).

Characterization of Pentacene Films. The pentacene films were deposited at a substrate temperature of 24 °C. AFM micrographs of 60 nm pentacene films on a silica surface predeposited with polyPDA films of various thicknesses are shown in Figure 5, with that on a bare silica surface included as a reference. On a bare silica surface, characteristic morphologies of dendritic crystallites were formed, with the grain sizes in the range of ~1 μm. The grains exhibited terraced structure with a step height of ca. 1.55 nm. Thus a herringbone molecular packing with the long molecular axis nearly perpendicular to the surface was obtained. On the surface with ~7 nm polyPDA deposited, where the surface was nearly all covered with polymer films of PDA dimers, much smaller grains were obtained, ranging

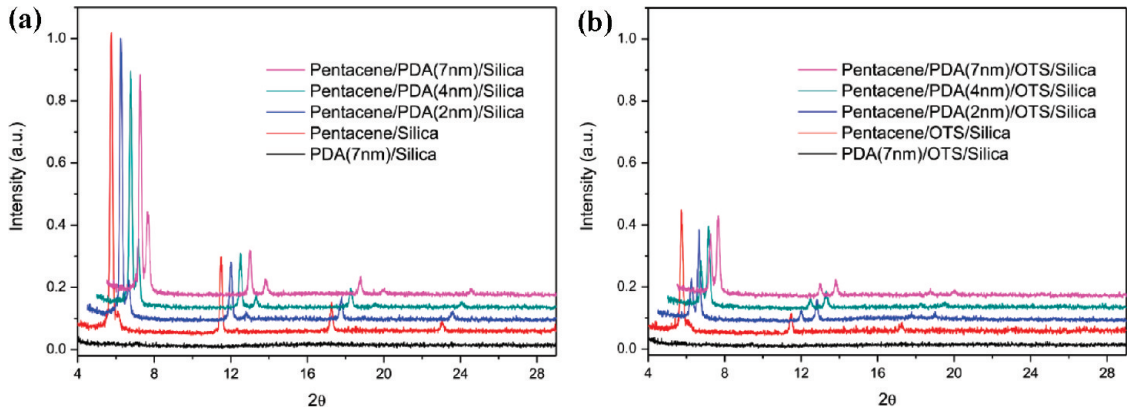

FIGURE 6. X-ray diffraction patterns for 60 nm pentacene films deposited on (a) polyPDA-decorated silica substrate and (b) OTS-modified silica that has polyPDA films on top, with a nominal polyPDA film thickness of 2, 4, and 7 nm, and on substrates without polyPDA films on top.

from 0.1 to 0.5 μm in size. The grains also exhibit terraced structure of similar step heights. Yet the shapes are irregular and clearly different from the apparent dendritic crystallites obtained on a bare silica surface. The film morphology is affected by both surface energy as well as roughness. A flat surface would favor larger grains because the molecules can migrate/diffuse readily without bumping into heterogeneities and nucleate. A lower energy surface, we contend, would also favor migration/diffusion of molecules on the surface because the interaction between the molecule and the surface is weaker, and thus larger grains will result (31). A bare silica surface is flat yet hydrophilic (higher surface energy), whereas the bilayer film-covered surface is rough yet hydrophobic (lower surface energy). The observed morphology suggests the dominant effect of surface roughness here. On a surface deposited with ~4 nm polyPDA films, clearly two types of morphologies were observed, one with larger grains similar to that deposited on the bare silica surface and the other similar to grains deposited on silica with 7 nm polyPDA present. The larger gains are believed to be grown on the bare silica regions and the smaller grains are on the dimer layer film regions on the surface.

AFM micrographs of 60 nm pentacene films deposited on OTS-modified silica surfaces decorated with polyPDA films of various nominal thicknesses are also shown in Figure 5. At low polyPDA coverage (~2 nm), the grains were much smaller than that on corresponding bare silica surface. This can be explained by a molecularly rough OTS-modified surface which induced smaller grain growth. On OTS-silica with 7 nm polyPDA film on the surface, the pentacene film contained small grains with numerous higher clusters (as high as 180 nm).

X-ray diffractions of the pentacene/polyPDA composite films were measured. Diffraction peaks at $2\theta = 5.8$, 11.5, 17.3, and 23.1°, assignable to the (001), (002), (003), and (004) diffraction peaks, respectively, for the thin film phase of pentacene, appeared on all substrates, with or without OTS-modification (32, 33). The thin film phase has an orthorhombic structure with layered and herringbone packing. The long molecular axes aligned nearly perpendicular to the substrate with an interlayer spacing of 1.54 nm. On bare silica-polyPDA surfaces, a small contribution of the bulk pentacene phase, with 2θ at 6.2 and 12.4° for (001′) and (002′), respectively, was also observed. The bulk phase was reported to have a triclinic structure with an interlayer spacing of 1.44 nm (34, 35). Contribution of the bulk phase increased with increasing amount of polyPDA on the substrate. On polyPDA-decorated, OTS-modified surface, the bulk phase was much more significant and even became dominant in the presence of 7 nm polyPDA films. The results are summarized in Figure 6.

Electrical Properties. Field-effect transistors were fabricated on the pentacene-PDA composite films in a bottom-gate, top-contact configuration by depositing gold source and drain electrodes through a shadow mask. Typical p-type behavior was observed in all cases (see Figure S4 in the Supporting Information). Nevertheless, the output current as well as the calculated field-effect mobility of the transistors showed a decreasing trend with increasing PDA thickness incorporated in the film.

When the current was measured at a constant source-drain bias of −50 V with the gate voltage swept from +100 V toward −100 V and back to +100 V again, a clear hysteresis was obtained. A higher current trace was followed when the gate bias was swept from +100 V toward −100 V and a low current trace was followed in the backward direction. The traces are repeatable. Thus a significant electric bistability appeared. The memory window, defined as the threshold voltage shift (ΔV_{th}) in the bisweeps of the gate voltage, increases with the nominal thickness of the polyPDA films, that is, a larger memory window with increasing polyPDA thickness underneath. Similar phenomena were observed for the devices prepared from pentacene/polyPDA films on bare silica (Figure 7a) or on OTS-modified silica surface (Figure 7b). There is some distinct difference between the shapes of the two, which will be addressed later. In contrast, the devices prepared on SiO_2 or OTS-modified SiO_2 without the polyPDA films present or on SiO_2 with deposited films of a saturated hydrocarbon (*n*-hexacosane) gave very little hysteresis. Thus the large hysteresis has to be related to the conjugated polyPDAs incorporated

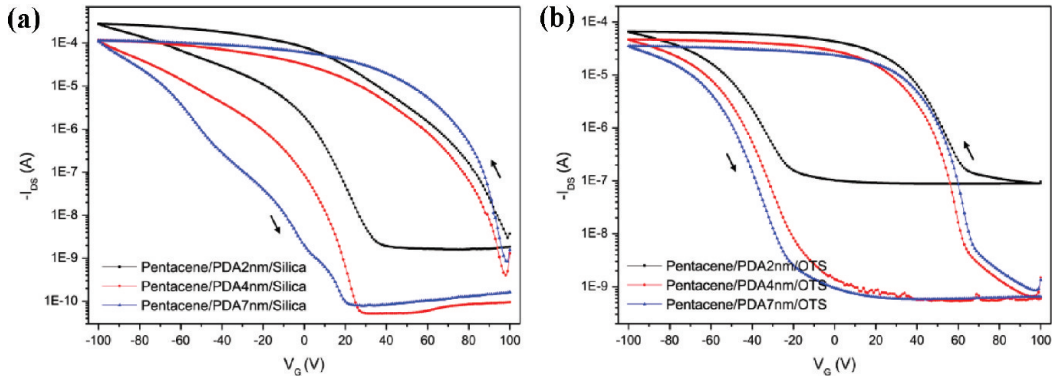

FIGURE 7. Transfer characteristics with bidirection scan of gate voltage as a function of the polyPDA thickness. (a) Devices prepared on bare silica surface; (b) devices prepared on OTS-modified silica surface. The V_{ds} was kept at −50 V, and the V_{gs} bias was swept from +100 V to −100 V and returned to +100 V again. The arrows indicate the direction of the V_{gs} sweep.

Table 1. Transistor/Memory Device Characteristics of the Pentacene/PolyPDA Composite Films

	V_{th} (V)		mobility			
	100 V to −100 V	−100 V to 100 V	100 V to −100 V	−100 V to 100 V	on−off ratio	memory window (V)
pentacene/silica	9.90	3.05	0.33	0.34	1×10^5	6.85
pentacene/PDA2 nm/silica	50.58	−22.40	0.55	0.74	1×10^5	72.98
pentacene/PDA4 nm/silica	61.74	−46.22	0.16	0.58	1×10^7	107.96
pentacene/PDA7 nm/silica	79.71	−70.72	0.22	2.08	1×10^7	150.43
pentacene/OTS/silica	−20.05	−27.07	0.83	0.83	1×10^7	7.02
pentacene/PDA2 nm/OTS	57.76	−31.74	0.40	0.40	1×10^3	89.50
pentacene/PDA4 nm/OTS	55.31	−36.78	0.23	0.25	1×10^5	92.09
pentacene/PDA7 nm/OTS	59.46	−41.48	0.22	0.23	1×10^5	100.94

in the pentacene film. The calculated mobility in each sweep direction, on/off ratio, and threshold shifts are summarized in Table 1.

Comparing the *I*−*V* hysteresis observed here with that obtained with pentacene film embedding gold nanoparticles (9), we suggest the mechanism to be the following: at positive gate bias, negative charges are trapped in polyPDA through pentacene from the source/drain electrodes (36, 37), whereas at negative bias, positive charges are trapped in polyPDA. The opposite charges trapped in the conjugated polymer create local electric fields which offset the gate bias and cause different shifts in the threshold voltages and thus different conductivities at the same bias. An analysis of the energy levels of related materials lends support of the mechanism. As shown in Figure 8, the HOMO/LUMO levels for polyPDA are about 5.2 and 3.4 eV respectively. The corresponding values for pentacene are 5.1 and 2.9 eV, respectively. The work function of Au is 5.0 eV. With positive bias, electron carriers accumulate in the LUMO of pentacene and then transport to the LUMO of polyPDA and are trapped there. Although the injection of electrons from gold into LUMO of pentacene involves a large barrier and appears difficult, ambipolar behavior of pentacene-based transistor with gold as source/drain has been well-documented (36, 37). Upon sweeping toward negative bias, the electrons are being detrapped or hole charges are getting into the polymer backbone. At −100 V, the polyPDA are charged only with holes. The charge transport between the HOMOs of pentacene and polyPDA are made feasible under the action of a gate bias.

The shifts in threshold voltages (memory window) reflect the ability of charge storage in the polyPDA. With more polyPDA at the interface, more charges can be trapped and a larger memory window resulted. The hysteresis also

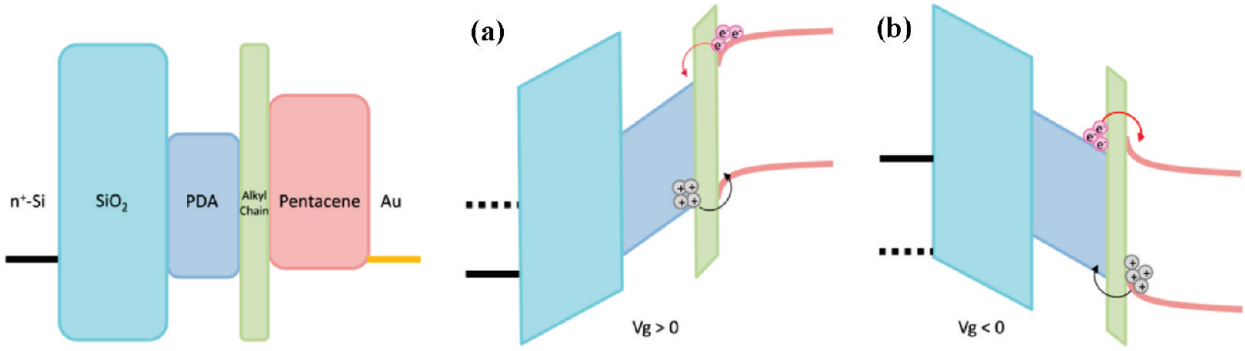

FIGURE 8. Schematic energy band diagrams of pentacene/PDA/silica/n^+-Si before gate bias (left) and under (a) a positive gate voltage, and (b) a negative gate voltage.

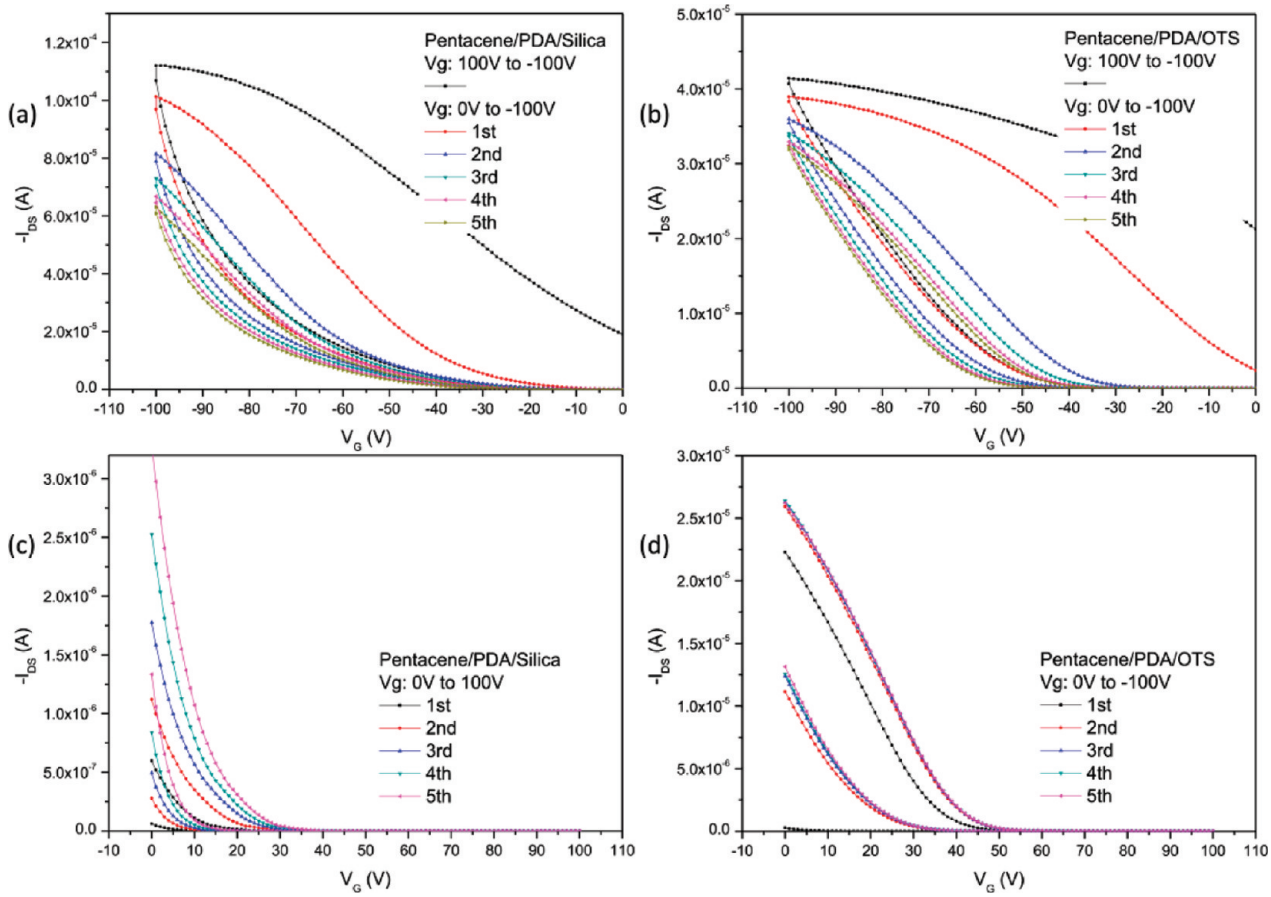

FIGURE 9. Transfer characteristics of the devices with pentacene/polyPDA on silica and on OTS-modified silica substrates. (a, b) Gate bias cycled between 0 and −100 V after initial scan from +100 to −100 V. (c, d) Gate bias cycled between 0 and +100 V after an initial from +100 to −100 V (not shown).

depends on scan ranges of the gate bias and the sweep rate. Increasing the bias sweeping range increases the memory window, a result attributable to more charges being trapped in the conjugated backbone at higher gate voltages. Higher positive bias shifts the threshold voltage to the positive direction and more negative bias shifts the threshold voltage negatively. The ability of polyPDA to trap either holes or electrons is important in expanding the memory window. This characteristics also suggest that the charge trapping occurs at the interfacial region rather than in the pentacene layer, because hysteresis due to traps in the semiconductor layer is not sensitive to gate bias change (4, 38). The trapping/detrapping behavior also depends on the sweeping rate. At a slower sweeping rate, more charges can be trapped and the memory window increases.

When the gate bias was cycling between 0 and −100 V after an initial scan from +100 V to −100 V, a shrinking hysteresis was obtained (Figure 9a, b). This process served to charge the conjugated backbones with holes in each cycle without discharging them with any positive bias. A steady negative shift in V_{th} was observed, more significant in the sweeps from 0 to −100 V (high conductivity state) than in the sweeps from −100 to 0 V (low conductivity state), resulting in a reduced hysteresis with each scan. For pentacene/polyPDA prepared on a bare silica substrate, where large ring patterns of polyPDA were formed, the current and hysteresis decreased with repetitive sweeps to eventually a converged curve. This indicates that each repetitive sweep toward −100 V increased some positive charges in the conjugated backbones to a final saturated state and the charges did not escape significantly during the sweep from −100 V to 0 V. On the other hand, for pentacene/polyPDA deposited on OTS-modified silica substrate, where evenly distributed but multilayered clusters of polyPDA were formed, the hysteresis stabilized and remained nearly constant after the third cycle. This suggests the charging (with holes) in the sweeps between 0 and −100 V and decharging (or loss of charges from the polyPDA system to relax the internal repulsion) in the sweeps from −100 V to 0 V reached an equilibrium so that a finite hysteresis was maintained. It should be noted that a voltage sweep to +100 V recovered the initial full hysteresis in both cases. These results imply that the device could be programmed (0 to −100 V) and erased (+100 to 0 V) repeatedly. Alternatively, when the gate bias was cycling between 0 and +100 V after the initial scan of the gate voltage from +100 to −100 V, distinct transfer characteristics were obtained (Figure 9c, d). This process served to input negative charges into the polyPDA system. Repeated cycles brought about increasingly positive shift of V_{th}, and increasing current and eventually stabilized. For pentacene/polyPDA deposited on a bare silica substrate, a steady increase in the current and a steady positive shift of V_{th} were obtained. This suggests more negative charges were trapped in the conjugated backbones in the sweep from 0 V

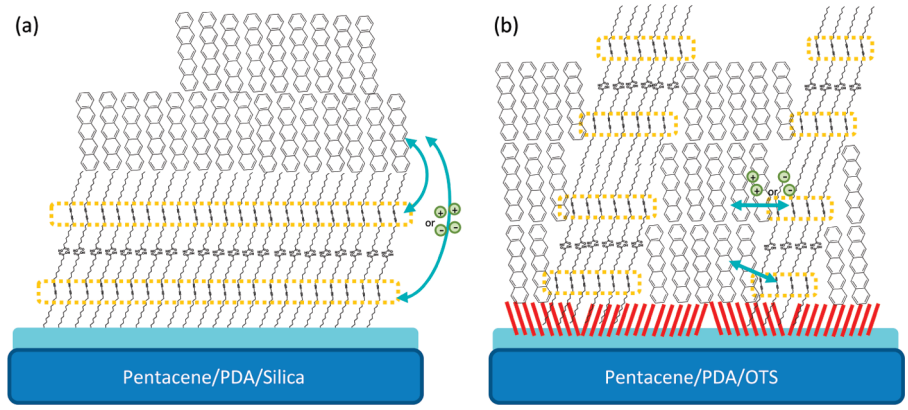

FIGURE 10. Schematic diagrams of the pentacene molecules deposited on (a) the polyPDA-covered silica substrate and (b) the polyPDA-covered OTS-modified silica substrate.

to +100 V, whereas the charge loss was not serious in the sweeps from +100 to 0 V. For pentacene/polyPDA deposited on OTS-modified silica, the hysteresis stabilized in the second cycle and remained nearly constant, implying that the trapping and detrapping of negative charges reached equilibrium after the second sweep. These results indicate that for the devices with pentacene/polyPDAs deposited on bare silica substrate, the charges were injected into the polyPDA less readily so that more charges were injected in each additional sweep. The system could nevertheless hold the charges better, so that fewer charges were lost with decreasing bias. For pentacene/polyPDA deposited on OTS-modified silica substrate, the charges were trapped more readily but also lost readily so that trapping and detrapping reach an equilibrium quickly and a finite hysteresis was maintained. The different behavior of the two systems has to do with the different morphology of the polyPDA films obtained. This will be addressed later.

The memory device can also be switched "on" and "off" by applying a positive gate bias pulse or negative gate bias pulse respectively and then the current is measured at 0 V gate bias. The "on" current showed a dependence on the pulse time, increasing with longer pulse time of positive bias. This can be rationalized as more negative charges being trapped with longer pulse. The "off" current decreased also with longer pulse time of the negative bias, because more positive charges were trapped (see Figure S5a in the Supporting Information).

The retention characteristics of the polyPDA-incorporated devices were also measured by recording the "on" (or "off") current at $V_g = 0$ V as a function of time after a +100 V (or −100 V) pulse. A gradual decay of the "on" current and a gradual back up of the "off" current were observed (see Figure S5b in the Supporting Information), presumably due to discharge of the polyPDA when the gate bias is removed. Reversible switching between high and low conductivity states is demonstrated by repeated programming (V_g = −100 V), reading (at $V_g = 0$ V, $V_{ds} = -50$ V), erasing V_g = 100 V), and reading ($V_g = 0$ V, $V_{ds} = -50$ V) (see Figure S6 in the Supporting Information). These write-read-erase cycles and the duration test exhibited by the devices with polyPDA-incorporated pentacene film are reasonably stable and hold the potential for use as nonvolatile memory.

A comparison of the $I-V$ hystereses in Figure 7 shows that pentacene/polyPDA film deposited on an OTS-modified silica substrate gave a steeper flank of hysteresis than that with the film deposited on bare silica substrate. This may imply a faster response of the trapping/detrapping process for pentacene/polyPDA film on the OTS-modified surface than on the bare silica surface. The two cases mainly differ in the morphology of the polyPDA films deposited. It is suggested that, on bare silica surface, the polyPDA formed rather extended ring patterns of dimer layer, and thus the surface distribution is less even and fewer molecular contacts between pentacene layers and the ene−yne conjugated system (with the alkyl chain matrix interposed as a barrier). On OTS-modified surface, smaller and more evenly distributed and steep clusters of multiple layers are formed, with more molecular contacts between pentacene layers and the conducting backbone. Charge transport between the pentacene layer and the polyPDA system is more facile. This also explains the less-sensitive pulse-time dependence of the "on" and "off" current and faster decay of the currents with reading time, as shown in Figure 10. The different behaviors observed when charging the systems with repetitive cycles between 0 and −100 V or 0 and +100 V can be understood in the same way. That is, the system with more molecular contacts between pentacene and the conjugated backbones has faster response in the trapping/detrapping processes so that the ultimate state is reached faster. Figure 10 depicts the proposed structure.

CONCLUSION

We demonstrated that a transistor/memory device based on pentacene film can be prepared by incorporating poly(10, 12-pentacosadiynoic acid, PDA), into the conducting channel, with the conjugated polydiacetylenes backbone acting as charge traps at the semiconductor/dielectric interface. Thermally evaporated PDA molecules self-assembled into unique patterns or clusters of H-bonded dimer layer, depending on the surface nature (hydrophilic, hydrophobic, smooth, or rough). Topochemical polymerization of the PDA moieties provides a vehicle to store charges when these polyPDAs were embedded into a pentacene film. The presence of these polymers has an impact on the morphology as well as crystalline phases of the pentacene films deposited

on top, resulting smaller grains and increasing bulk phase contribution. Nevertheless, highly efficient field-effect transistors are achieved. The polyPDAs serve as floating gate through charge-trapping in the conjugated backbones. IV hysteresis and thus electric bistability are observed with the memory window, on/off ratio and retention time of the memory device related to the amount of charges that can be trapped and retained. The structure/property correlation provides further insights for developing new and improved transistor/memory devices for practical applications.

Acknowledgment. The authors thank the National Science Council of Taiwan, the Republic of China, and Academia Sinica for financial support of this work.

Supporting Information Available: Some characterization data and device characteristics (PDF). This material is available free of charge via the Internet at http://pubs.acs.org.

REFERENCES AND NOTES

(1) Dimitrakopoulos, C. D.; Malenfant, P. R. L. *Adv. Mater.* **2002**, *14*, 99.
(2) Yang, Y.; Ouyang, J.; Ma, L. P.; Tseng, R. J. H.; Chu, C. W. *Adv. Funct. Mater.* **2006**, *16*, 1001.
(3) Naber, R. C. G.; Asadi, K.; Blom, P. W. M.; Leeuw, D. M. D.; Boer, B. D. *Adv. Mater.* **2009**, *22*, 933.
(4) Wu, W.; Zhang, H.; Wang, Y.; Ye, S.; Guo, Y.; Di, C.; Yu, G.; Zhu, D.; Liu, Y. *Adv. Funct. Mater.* **2008**, *18*, 2593.
(5) Faber, H.; Burkhardt, M.; Jedaa, A.; Kälblein, D.; Klauk, H.; Halik, M. *Adv. Mater.* **2009**, *21*, 3099.
(6) Leong, W. L.; Lee, P. S.; Lohani, A.; Lam, Y. M.; Chen, T.; Zhang, S.; Dodabalapur, A.; Mhaisalkar, S. G. *Adv. Mater.* **2008**, *20*, 2325.
(7) Leong, W. L.; Lee, P. S.; Mhaisalkar, S. G. *Appl. Phys. Lett.* **2007**, *90*, 042906.
(8) Novembre, C.; Guérin, D.; Lmimouni, K.; Gamrat, C.; Vuillaume, D. *Appl. Phys. Lett.* **2008**, *92*, 103314.
(9) Tseng, C. W.; Tao, Y. T. *J. Am. Chem. Soc.* **2009**, *131*, 12441.
(10) Wang, S. M.; Leung, C. W.; Chan, P. K. L. *Org. Electron.* **2010**, *11*, 990.
(11) Schmidt, G. M. J. *Solid State Photochemistry*. Verlag Chemie: Weinheim, Germany, 1976.
(12) Baba, K.; Kasai, H.; Shinohara, Y.; Okada, S.; Oikawa, H.; Matsuda, H.; Nakanishi, H. *Jpn. J. Appl. Phys.* **2008**, *47*, 3769.
(13) Yoon, B.; Lee, S.; Kim, J. M. *Chem. Soc. Rev.* **2009**, *38*, 1958.
(14) Nishide, J. I.; Oyamada, T.; Akiyama, S.; Sasabe, H.; Adachi, C. *Adv. Mater.* **2006**, *18*, 3120.
(15) Koyanagi, T.; Muratsubaki, M.; Hosoi, Y.; Shibata, T.; Tsutsui, K.; Wada, Y.; Furukawa, Y. *Chem. Lett.* **2006**, *35*, 20.
(16) Chen, L. W.; Ludeke, R.; Cui, X. D.; Schrott, A. G.; Kagan, C. R.; Brus, L. E. *J. Phys. Chem. B* **2005**, *109*, 1834.
(17) Kim, J. M.; Lee, Y. B.; Chae, S. K.; Ahn, D. J. *Adv. Funct. Mater.* **2006**, *16*, 2103.
(18) Lifshitz, Y.; Golan, Y.; Konovalov, O.; Berman, A. *Langmuir* **2009**, *25*, 4469.
(19) Narita, Y.; Tadokoro, T.; Ikeda, T.; Saiki, T.; Mononobe, S.; Ohtsu, M. *Appl. Spectrosc.* **1998**, *52*, 1141.
(20) Galiotis, C.; Young, R. J.; Batchelder, D. N. *J. Mater. Sci. Lett.* **1983**, *2*, 263.
(21) Ulman, A.; Eilers, J. E.; Tillman, N. *Langmuir* **1989**, *5*, 1147.
(22) Shtein, M.; Mapel, J.; Benziger, J. B.; Forrest, S. R. *Appl. Phys. Lett.* **2002**, *81*, 268.
(23) Yang, S. Y.; Shin, K.; Park, C. E. *Adv. Funct. Mater.* **2005**, *15*, 1806.
(24) Dimitrakopoulos, C. D.; Brown, A. R.; Pomp, A. *J. Appl. Phys.* **1996**, *80*, 2501.
(25) Yagi, I.; Tsukagoshi, K.; Aoyagi, Y. *Appl. Phys. Lett.* **2005**, *86*, 103502.
(26) Di, C. A.; Yu, G.; Liu, Y. Q.; Guo, Y. L.; Sun, X. N.; Zheng, J.; Wen, Y. G.; Wang, Y.; Wu, W. P.; Zhu, D. B. *Phys. Chem. Chem. Phys.* **2009**, *11*, 7268.
(27) Lee, H. S.; Kim, D. H.; Cho, J. H.; Hwang, M.; Jang, Y.; Cho, K. *J. Am. Chem. Soc.* **2008**, *130*, 10556.
(28) Virka, A.; Mannsfeld, S.; Oh, J. H.; Toney, M. F.; Tan, Y. H.; Liu, G. Y.; Scott, J. C.; Miller, R.; Bao, Z. *Adv. Funct. Mater.* **2009**, *19*, 1962.
(29) Tillman, N.; Ulman, A.; Schildkraut, J. S.; Penner, T. L. *J. Am. Chem. Soc.* **1988**, *110*, 6136.
(30) Knipp, D.; Street, R. A.; Völkel, A.; Ho, J. *J. Appl. Phys.* **2003**, *93*, 347.
(31) Weidkamp, K. P.; Tromp, R. M.; Hamers, R. J. *J. Phys. Chem. C* **2007**, *111*, 16489.
(32) Hu, W. S.; Tao, Y. T.; Hsu, Y. J.; Wei, D. H.; Wu, Y. S. *Langmuir* **2005**, *21*, 2260.
(33) Fritz, S. E.; Martin, S. M.; Frisbie, C. D.; Ward, M. D; Toney, M. F. *J. Am. Chem. Soc.* **2004**, *126*, 4084.
(34) Drummy, L. F.; Martin, D. C. *Adv. Mater.* **2005**, *17*, 903.
(35) Cheng, H. L.; Mai, Y. S.; Chou, W. Y.; Chang, L. R.; Liang, X. W. *Adv. Funct. Mater.* **2007**, *17*, 3639.
(36) Heim, T.; Lmimouni, K.; Vuillaume, D. *Nano Lett.* **2004**, *4*, 2145.
(37) Singh, T. B.; Meghdadi, F.; Günes, S.; Marjanovic, N.; Horowitz, G.; Lang, P.; Bauer, S.; Sariciftci, N. S. *Adv. Mater.* **2005**, *17*, 2315.
(38) Park, C. B.; Yokoyama, T.; Nishimura, T.; Kita, K.; Toriumi, A. *Jpn. J. Appl. Phys.* **2008**, *47*, 3189.

AM100696V